J Mater Sci (2009) 44:2031–2037
DOI 10.1007/s10853-009-3285-2

Electrical conduction in $La_{0.9}Ba_{0.1}Er_{1-x}Mg_xO_{3-\alpha}$ ceramics

Qing Yang · Yingxin Guo · Baoxin Liu · Cheng Chen · Wenbao Wang · Guilin Ma

Received: 10 September 2008 / Accepted: 20 January 2009 / Published online: 20 February 2009

Abstract Doubly doped $LaErO_3$ ceramics, $La_{0.9}Ba_{0.1}Er_{1-x}Mg_xO_{3-\alpha}$ (x = 0.05, 0.10, 0.15, 0.20), were synthesized by solid-state reaction method and characterized by X-ray diffraction (XRD). The samples have a single orthorhombic perovskite-type structure. The conduction behavior was investigated using various electrochemical methods including AC impedance spectroscopy, gas concentration cell, isotope effect of hydrogen, and hydrogen electrochemical permeation (pumping) in the temperature range of 500–1000 °C. The results indicated that specimens were pure ionic conductors under low oxygen partial pressure (about 10^{-7}–10^{-20} atm) and mixed conductors of proton, oxide ion, and electron hole under high oxygen partial pressure (about 10^{-5}–1 atm). The pure ion conduction of the ceramics in hydrogen atmosphere was confirmed by electromotive force method of hydrogen concentration cell, and the observed emf values coincided well with the theoretical ones. The conductivity in H_2O–Ar atmosphere was higher than that in D_2O–Ar atmosphere, exhibiting an obvious isotope effect and proton conduction in water vapor containing atmosphere. It has been confirmed by electrochemical hydrogen permeation (hydrogen pumping) experiment that the ceramics were mainly proton conductors in hydrogen containing atmosphere. Whereas in dry oxygen-containing atmosphere, observed emf values of the oxygen concentration cell were far lower than the theoretical ones, indicating that the ceramics were mixed conductors of electron hole and oxide ion.

Q. Yang · Y. Guo · B. Liu · C. Chen · W. Wang · G. Ma (✉)
Key Laboratory of Organic Synthesis of Jiangsu Province, College of Chemistry, Chemical Engineering and Materials Science, Suzhou University, Suzhou 215123, People's Republic of China
e-mail: 32uumagl@suda.edu.cn

Introduction

Since the discovery of high temperature (600–1000 °C) proton conduction in doped perovskite-type $SrCeO_3$ [1] by Iwahara et al. in 1981, a number of materials such as doped $BaCeO_3$ [2], $AZrO_3$ (A = Ca, Sr, Ba) [3], $Ba_3Ca_{1+x}Nb_{2-x}O_9$ [4], $LaErO_3$ [5], Ln_2ZrO_7 [6], $Ba_2SnYO_{5.5}$ [7], $LaScO_3$ [8], and $LaGaO_3$ [9] have been found to exhibit appreciable proton conduction. High temperature proton conduction has attracted considerable attention due to their increasing importance for potential applications [10–12] in hydrogen sensors, solid oxides fuel cell (SOFC), water electrolysis, separation and purification of hydrogen, hydrogenation, and dehydrogenation of some organic compounds, synthesis of ammonia at atmospheric pressure, membrane reactors, and other high temperature electrochemical devices.

In 1994, Norby [5] synthesized the ceramic specimens of $La_{0.9}M_{0.1}ErO_3$ (M = Ca^{2+}, Sr^{2+}, Ba^{2+}) and $LaEr_{0.9}Ca_{0.1}O_3$, in which Sr^{2+}, Ba^{2+} were doped on the La^{3+} site, while Ca^{2+} doped both on the La^{3+} and Er^{3+} sites. The doped $LaErO_3$ has been found to be a nearly pure proton conductor at low temperature and high water vapor pressure. The activation energy for proton conduction decreases with the increase of ion radius of dopant M in $La_{0.9}M_{0.1}ErO_3$ (M = Ca^{2+}, Sr^{2+}, Ba^{2+}). In recent years, there were almost no reports about the conduction behaviors of doped $LaErO_3$, especially, no reports on doubly doped both on the La^{3+} and Er^{3+} sites of $LaErO_3$.

In this article, the doubly doped ceramic specimens by Mg^{2+} and Ba^{2+}, $La_{0.9}Ba_{0.1}Er_{1-x}Mg_xO_{3-\alpha}$ (x = 0.05, 0.10, 0.15, 0.20) were synthesized by the conventional solid-state reaction method, and the transport behavior in the specimens was investigated using various electrochemical methods including AC impedance spectroscopy, gas

concentration cell, isotope effect of hydrogen, and hydrogen electrochemical permeation (pumping).

Experimental

$La_{0.9}Ba_{0.1}Er_{1-x}Mg_xO_{3-\alpha}$ ($x = 0.05$, 0.10, 0.15, 0.20) ceramics were prepared by the conventional solid-state reaction method. The required amounts of La_2O_3 (99.99%), $Ba(CH_3COO)_2$ (99.99%), Er_2O_3 (99.9%), and MgO (99.99%) reagents were fully mixed in an agate mortar for 1 h with ethanol and dried by an infrared lamp. The mixed powders were calcined at 1200 °C for 10 h in air. The obtained oxides were ground in an agate mill container with ethanol and agate balls using a planetary ball mill machine at 150 revolutions per minute for 2 h, and then dried by an infrared lamp, followed by sieving (100 mesh). The resulting powder was pressed into pellets (diameter 18 mm, thickness 2 mm) by a hydrostatic pressure of 2×10^8 Pa, and sintered at 1300–1500 °C in air for 10 h. The ceramics thus obtained were made into thin discs with the diameter of 13 mm and the thickness of 0.6 mm to serve as electrolytes for the electrochemical determinations.

The structural characteristics of the ceramic specimens were determined at room temperature by powder X-ray diffraction analysis using a nickel filtered Cu K (λ = 0.15405 nm) radiation (Panatytical X' Pert Pro MPD X-ray diffractometer). The scanning range and scanning rate were 20°–80° and 2.00° min^{-1}, respectively.

The conductivity of ceramic specimens was measured by an AC impedance method over the frequency range 1 Hz–3 MHz using electrochemical workstations (German ZAHNER IM6ex) in the temperature range of 500–1000 °C under the atmospheres of air, wet air, wet hydrogen, H_2O–Ar, and D_2O–Ar. The conductivity as the function of oxygen partial pressure p_{O_2} was measured in the p_{O_2} range of 1–10^{-20} atm. The p_{O_2} was accommodated by mixing O_2, air, Ar, and H_2 in proper ratio, and measured using a YSZ oxygen sensor on line.

The ionic transport numbers in different atmosphere were obtained by gas concentration cells using the ceramic specimen as an electrolyte diaphragm in the temperature range of 500–1000 °C. For all electrochemical measurements, porous platinum electrodes were used onto two faces of the discs, and platinum mesh was used as the current collector. In order to determine ionic transport numbers in hydrogen, dry oxygen-containing atmospheres and wet air, the following hydrogen, oxygen, and water vapor concentration cells were constructed:

wet H_2, $Pt|La_{0.9}Ba_{0.1}Er_{1-x}Mg_xO_{3-\alpha}|Pt$, wet H_2-Ar

dry air, $Pt|La_{0.9}Ba_{0.1}Er_{1-x}Mg_xO_{3-\alpha}|Pt$, dry O_2

wet air (30 °C), $Pt|La_{0.9}Ba_{0.1}Er_{1-x}Mg_xO_{3-\alpha}|Pt$, wet air (0 °C)

The partial pressure of hydrogen gas, p_{H_2}, was accommodated by mixing high pure hydrogen (99.999%) and high pure argon (99.999%) using a gas blender. Wet gas was obtained by bubbling through water, and dry gas was obtained by drying through P_2O_5. Specially, the water vapor partial pressure in both chambers of hydrogen concentration cell was kept constant ($p_{H_2O} = 0.023$ atm at 20 °C). The electromotive forces of the gas concentration cell, E_{obs}, were measured in the temperature range of 500–1000 °C, and the ionic transport numbers were calculated as

$$t_i = \frac{E_{obs}}{E_{cal}} \quad (1)$$

where E_{cal} is the theoretical value calculated from the Nernst equation.

To verify the proton conduction in the ceramic specimen directly, we examined the electrochemical hydrogen permeation (hydrogen pumping) through the specimen by sending a direct current to the following electrolytic cell, in which $La_{0.9}Ba_{0.1}Er_{1-x}Mg_xO_{3-\alpha}$ was used as the electrolyte, and hydrogen and argon (carrier gas) were supplied to the anode and cathode chambers, respectively.

$(-)$ dry Ar, $Pt|La_{0.9}Ba_{0.1}Er_{1-x}Mg_xO_{3-\alpha}|Pt$, H_2 $(+)$

In order to avoid the influence of electrolysis of water vapor in argon, argon gas was dried by flowing argon gas through a cold trap based on low temperature nitrogen gas (about −120 °C). If the specimen was a proton conductor, the following electrode reactions would arise, when sending a direct current to the electrolytic cell.

$$\text{anode: } H_2 \rightarrow 2H^+ + 2e^- \quad (2)$$

$$\text{cathode: } 2H^+ + 2e^- \rightarrow H_2 \quad (3)$$

The protons produced by reaction (2) on the anode were transported through the sample to the cathode and turned into hydrogen gas molecules again. The generated hydrogen gas along with argon was carried into a hydrogen detector (Shanghai Gainforce SG33A) where the concentration of hydrogen gas in the mixed gases can be determined. Protonic transport number could be obtained by the ratio of the observed values versus theoretical ones which can be calculated according to the literature [9]. The flowing rate of argon was 30 mL/min during the experiment.

Results and discussion

Figure 1 shows the powder X-ray diffraction (XRD) patterns at room temperature of $La_{0.9}Ba_{0.1}Er_{1-x}Mg_xO_{3-\alpha}$ ($x = 0.05$, 0.10, 0.15, 0.20) ceramics. It is evident that

there are no additional peaks occurring in the patterns corresponding to the samples with $x = 0.05$, 0.10, 0.15, 0.20, all of the samples belong to a single phase of perovskite-type $LaErO_3$ orthorhombic system.

Figure 2 shows Arrhenius plots of the total conductivities of $La_{0.9}Ba_{0.1}Er_{1-x}Mg_xO_{3-\alpha}$ in three different atmospheres. The plots of each sample in the same atmosphere are similar. Specimens are mixed oxygen vacancy, proton and electron hole conductors, and variation of the plots is closely associated with temperature and contribution of partial conductivity of the charge carriers to the overall conductivity [5]. The form of the Arrhenius plot in air is analogous to that of $La_{0.9}Ba_{0.1}ErO_3$ in wet air [5]. In air, under about 700 °C, the overall conductivity increases in the order: $x = 0.15 > x = 0.10 > x = 0.05 > x = 0.20$, the specimen of $x = 0.15$ exhibits the highest conductivity among the specimens examined, which is similar to the order in wet H_2, according to the dominated status of proton at low temperature. However, there is very little difference from the overall conductivity of the specimens above 700 °C. The variation in the conductivities may be attributed to the effective concentration of oxygen vacancy in the specimens. On one hand, owing to the doping level of Ba^{2+} at La^{3+} sites is fixed, the total concentration of oxygen vacancy $V_O^{\bullet\bullet}$ mainly increases with the increasing of the doping level of Mg^{2+} at Er^{3+} sites. On the other hand, the concentrations of point defect pairs, $(Mg'_{Er} - V_O^{\bullet\bullet})$ and $(V_O^{\bullet\bullet} - Mg'_{Er} - V_O^{\bullet\bullet})$, which result from the coulombic attraction existing among the point defects with opposite charges, also increase at the same time, but this may reduce the total concentration of oxygen vacancy. Considering the two factors above, the effective concentration of oxygen vacancy reaches its highest value in $La_{0.9}Ba_{0.1}Er_{0.95}Mg_{0.05}O_{3-\alpha}$, in result the specimen of $x = 0.05$ exhibits the highest conductivity above 700 °C compared with others. It can be seen from Fig. 2a that an increase in slope of the Arrhenius plot occurs above 700 °C, which may be due to the boosting up of electron hole conductivity [7] in accordance with the increasing of electron hole transport number calculated from Fig. 7. In wet air (Fig. 2b), at 700–850 °C, the increasing extent of the total conductivity falls with the temperature rising compared with Fig. 2a. This variation perhaps arises from the decreasing of proton concentration. However, it arises again above 850 °C, perhaps by reason of the increasing contribution of electron holes partial conductivity. In wet H_2 (Fig. 2c), in analogy to oxide ionic conduction in air, the effective concentrations of $V_O^{\bullet\bullet}$ and $OH_O^{\bullet}$, which determine the proton conductivity of specimen, may be determined by the opposite factors below. On one hand, the increasing of doping level of Mg^{2+} at Er^{3+} sites is favorable for the increasing of effective concentrations of $V_O^{\bullet\bullet}$ and $OH_O^{\bullet}$, on the other hand, the concentrations of these point defect pairs $(Mg'_{Er} - V_O^{\bullet\bullet})$, $(V_O^{\bullet\bullet} - Mg'_{Er} - V_O^{\bullet\bullet})$, and $(Mg'_{Er} - OH_O^{\bullet})$, which result in the decreasing of effective concentrations of $V_O^{\bullet\bullet}$and $OH_O^{\bullet}$, also increase at the same time. Therefore, the conductivity increases in the order: $x = 0.15 > x = 0.10 > x = 0.05 > x = 0.20$. The specimen of $x = 0.15$ showed the highest conductivity (4.3×10^{-3} Scm^{-1} at 1000 °C), which was also higher than the conductivity (8.8×10^{-4} Scm^{-1} at 1000 °C) of $La_{0.9}Ba_{0.1}ErO_3$ [5] in wet hydrogen.

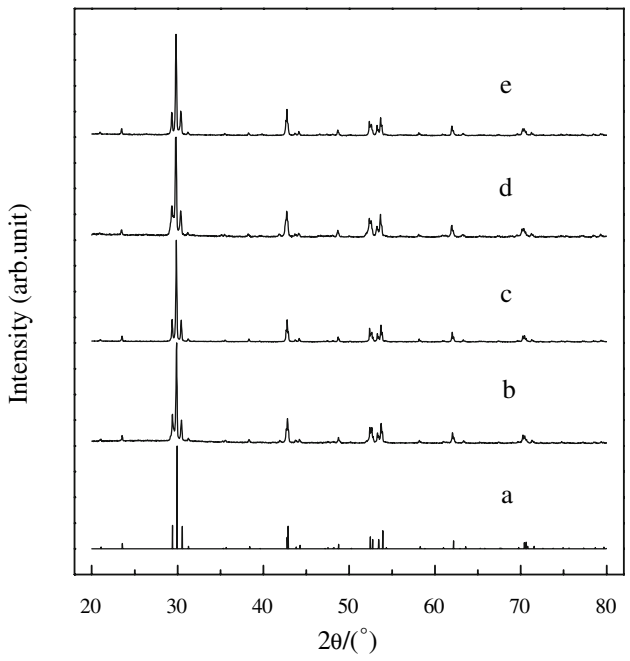

Fig. 1 XRD patterns of $La_{0.9}Ba_{0.1}Er_{1-x}Mg_xO_{3-\alpha}$ ceramics (a) JCPDS 72-0798; (b) $x = 0.05$; (c) $x = 0.10$; (d) $x = 0.15$; (e) $x = 0.20$

Figure 3 shows the Arrhenius plots of the total conductivities of $La_{0.9}Ba_{0.1}Er_{0.85}Mg_{0.15}O_{3-\alpha}$ in air, wet air, and wet H_2. The total conductivity for different atmospheres proceeds in the order: air > wet air > wet H_2. This tendency was also observed in all other specimens examined. This may be explained by the defect equilibrium chemistry expressed below [13–15]:

$$V_O^{\bullet\bullet} + \frac{1}{2}O_2 = O_O^{\times} + 2h^{\bullet} \quad (4)$$

$$H_2O(g) + 2O_O^{\times} + 2h^{\bullet} = 2OH_O^{\bullet} + \frac{1}{2}O_2 \quad (5)$$

$$H_2O(g) + O_O^{\times} + V_O^{\bullet\bullet} = 2OH_O^{\bullet} \quad (6)$$

$$\frac{1}{2}H_2 + O_O^{\times} = OH_O^{\bullet} + e' \quad (7)$$

where $V_O^{\bullet\bullet}$, $O_O^{\times}$, $OH_O^{\bullet}$, and $h^{\bullet}$are oxygen vacancy, oxide ion at normal lattice site, proton and electron hole, respectively. In air, due to the existence of oxygen molecules in air and oxygen vacancies in sample, some electron holes can be produced, based on the equilibrium reaction (4).

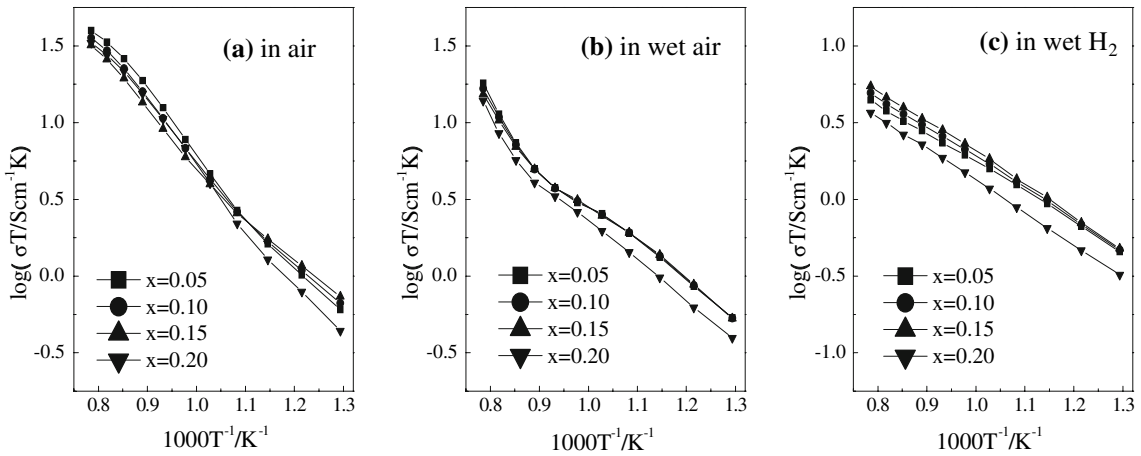

Fig. 2 Temperature dependence of electrical conductivity of $La_{0.9}Ba_{0.1}Er_{1-x}Mg_xO_{3-\alpha}$ ($x = 0.05, 0.10, 0.15, 0.20$) in **a** air, **b** wet air, and **c** wet hydrogen

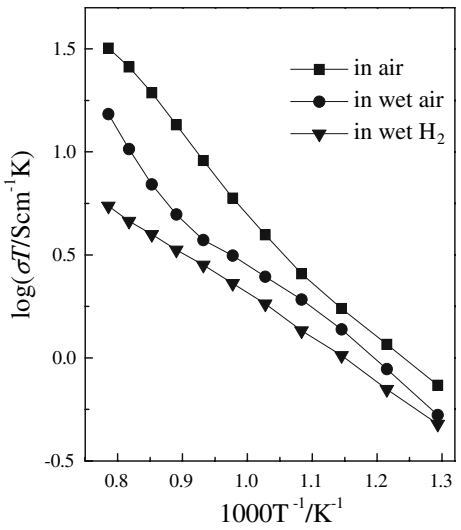

Fig. 3 Arrhenius plots of electrical conductivity of $La_{0.9}Ba_{0.1}Er_{0.85}Mg_{0.15}O_{3-\alpha}$ under different atmospheres

When water vapor and hydrogen are introduced, the contribution of electron hole and oxygen vacancy conduction decreases and proton conduction appears, according to the reaction (5), (7), and (6) which is the sum of reaction (4) and (5) and probably never takes place in a single step. The lower conductivity in wet air and H_2 containing atmosphere than in air originates in this reason. Furthermore, because the equilibrium reaction (7) is less favored [16], the lowest conductivity occurs in H_2 gas atmosphere in present study. In low temperature range (500–800 °C), the activation energies in air, wet air, and wet H_2 were 0.59, 0.47, and 0.43 eV, and in high temperature range (850–1000 °C), they were 0.71, 0.93, and 0.40 eV, respectively. The result of activation energies in wet H_2 are very close to the values of singly doped $LaErO_3$ reported by Norby [5]. The low temperature activation energies are typical activation energies of proton transport, and the high temperature activation energy (0.40 eV) in wet H_2 is slightly lower than the typical activation energies. This may be caused by many reasons, one of which may be the dehydration effect. As can be seen from the reaction (6), the equilibrium moves to the left hand with the temperature increasing, resulting that the proton concentration in the sample falls and the conductivity decreases as well in wet hydrogen.

An isotope effect on the conductivity of $La_{0.9}Ba_{0.1}Er_{1-x}Mg_xO_{3-\alpha}$ when using D_2O–Ar instead of H_2O–Ar as atmosphere was observed. As shown in Fig. 4, at all temperatures, the conductivity in H_2O–Ar atmosphere is higher than that in D_2O–Ar atmosphere. The increase in bulk resistance under D_2O–Ar atmosphere may be attributed to the decrease in mobility of the charge carrier, hydroxyl group ($OD_O^{\bullet}$). On one hand, the activation energy in low temperature region is different from that in high temperature region in H_2O–Ar or D_2O–Ar atmosphere, therefore pre-exponential factor, A_D or A_H, is different in low and high temperature region. The ratio of A_D/A_H is equal to 1.433 in high temperature region (850–1000 °C) and 1.336 in low temperature region (500–800 °C), the average value of the ratio is 1.39 which is close to the theoretical one [17]. On the other hand, when D_2O was in place of H_2O, the average activation energy for conduction increased 0.043 eV. This value is close to 0.05 eV, the difference in zero-point energy between O–H and –D bonds [18]. The isotope effect indicates that $La_{0.9}Ba_{0.1}Er_{1-x}Mg_xO_{3-\alpha}$ possesses proton conduction.

The representative relationship between electromotive force (EMFs) of hydrogen concentration cell based on $La_{0.9}Ba_{0.1}Er_{0.85}Mg_{0.15}O_{3-\alpha}$ and the hydrogen partial pressure (p_{H_2}) at 500–1000 °C is displayed in Fig. 5. The solid symbols ▶, ●, ▼, ▲, ◀ and ■ represent the observed EMFs (E_{obs}) at 500, 600, 700, 800, 900, and 1000 °C,

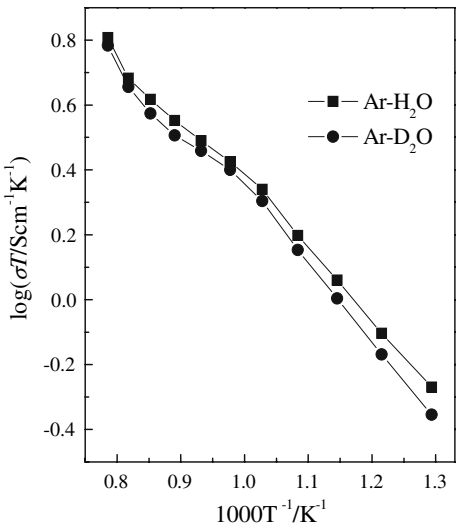

Fig. 4 Isotope effect on the conductivity of $La_{0.9}Ba_{0.1}Er_{0.85}Mg_{0.15}O_{3-\alpha}$

respectively. The dash line stands for the theoretical EMF (E_{cal}) calculated from Nernst equation at each temperature. According to the literature [19], if the specimen is a proton conductor and p_{H_2O} in both cell chambers is the same, E_{cal} can be obtained from the following Nernst equation.

$$E_{cal} = \frac{RT}{2F} \ln \frac{p_{H_2}(II)}{p_{H_2}(I)} \quad (8)$$

where $p_{H_2}(I)$ and $p_{H_2}(II)$ represent the hydrogen partial pressures in cathode and anode chamber, respectively, $p_{H_2}(II) > p_{H_2}(I)$, whereas R, T, and F have their usual meanings.

As shown in Fig. 5, each E_{obs} is well coincident with the corresponding E_{cal}, and the relationship between the E_{obs}

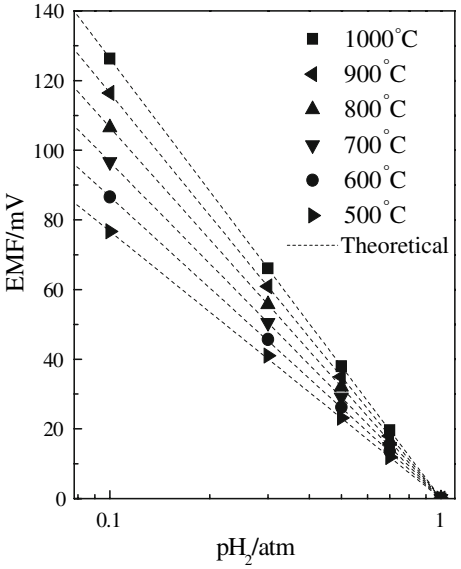

Fig. 5 EMFs of hydrogen concentration cell: wet H_2, Pt|$La_{0.9}Ba_{0.1}Er_{0.85}Mg_{0.15}O_{3-\alpha}$|Pt, wet H_2 − Ar

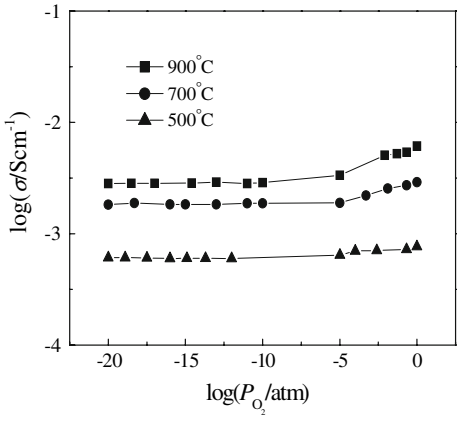

Fig. 6 Dependence of conductivity of $La_{0.9}Ba_{0.1}Er_{0.85}Mg_{0.15}O_{3-\alpha}$ on oxygen partial pressure

and the logarithm of p_{H_2} is linear. The ionic transport number, t_i, which can be determined from $E_{obs}/E_{cal} = t_i$, is almost unity at temperatures from 500 to 1000 °C in hydrogen atmosphere, indicating that the conductivity in hydrogen atmosphere shown in Fig. 2 is pure ionic conductivity. This is also in accordance with the conductivity measurements at low oxygen partial pressure range as shown in Fig. 6.

Similarly, the oxide ion conduction under higher oxygen partial pressure was studied by oxygen concentration cell method at temperature from 500 to 1000 °C. The representative EMF results of the concentration cell and oxide ionic transport number based on $La_{0.9}Ba_{0.1}Er_{0.85}Mg_{0.15}O_{3-\alpha}$ are shown in Fig. 7. The solid symbol stands for the observed EMFs (E_{obs}), the dash line represents the theoretical EMFs (E_{cal}) calculated from the following Nernst equation assuming that the transport number of oxide ion is unity at each temperature:

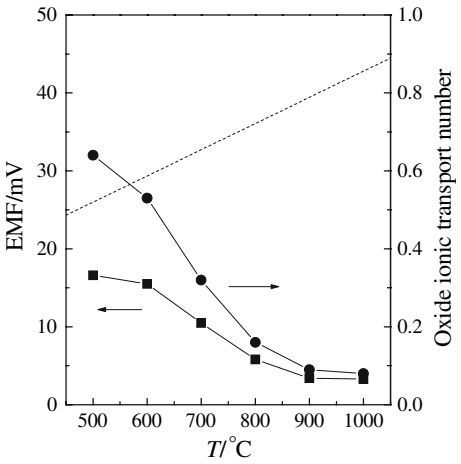

Fig. 7 EMFs (■) of oxygen concentration cell: dry air, Pt|$La_{0.9}Ba_{0.1}Er_{0.85}Mg_{0.15}O_{3-\alpha}$|Pt, dry O_2 and oxide ionic transport number (●) of the specimen

$$E_{\text{cal}} = \frac{RT}{4F} \ln \frac{p_{O_2}(\text{II})}{p_{O_2}(\text{I})} \tag{9}$$

where $p_{O_2}(\text{I})$ and $p_{O_2}(\text{II})$ are oxygen partial pressures in anode and cathode chambers, respectively. It can be seen from Fig. 7 that the concentration cell displays smaller EMF values than the theoretical ones, indicating that the specimen exhibits electron hole conduction to a great extent besides oxide ion conduction in dry air. From Eq. 1, the obtained oxide ionic transport numbers at 500, 600, 700, 800, 900, and 1000 °C are 0.64, 0.53, 0.32, 0.16, 0.09, and 0.08, respectively. Obviously, the oxide ion conduction decreased and the electron hole conduction increased as the temperature rising, which was consistent with the variety of conduction under oxidizing atmospheres as shown in Figs. 2 and 6.

The proton conduction in water vapor containing air was investigated by the steam concentration cell. Figure 8 shows the observed EMF results (E_{obs}) of the water vapor concentration cell and protonic transport number in wet air, the dash line stands for the theoretical EMF (E_{cal}) calculated from Nernst equation below:

$$E_{\text{cal}} = \frac{RT}{2F} \ln \frac{p_{H_2O}(30\ ^\circ\text{C})}{p_{H_2O}(0\ ^\circ\text{C})} \tag{10}$$

where p_{H_2O} (30 °C) and p_{H_2O} (0 °C) are water vapor partial pressures in air saturated at 30 °C and 0 °C, respectively. The protonic transport numbers in wet air are calculated from Eq. 1 to be 0.38 (500 °C), 0.27 (600 °C), 0.15 (700 °C), 0.07 (800 °C), 0.03 (900 °C), and 0.01 (1000 °C), respectively. It is obvious that the protonic transport number falls with temperature rising notably. This may be ascribed to the release of water vapor from the specimen and the decrease of proton concentration in the specimen as described by reaction (6), resulting in the decrease of protonic transport number.

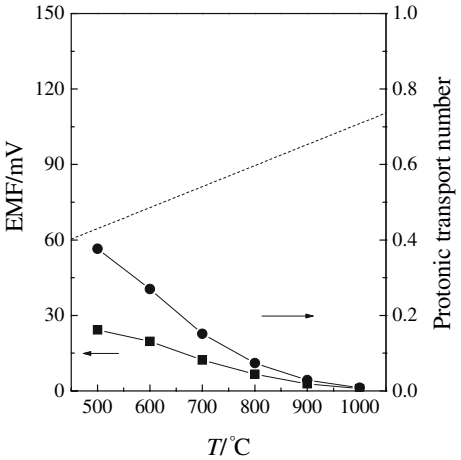

Fig. 8 EMFs (■) of the steam concentration cell: wet air (30 °C), Pt|$La_{0.9}Ba_{0.1}Er_{0.85}Mg_{0.15}O_{3-\alpha}$|Pt, wet air (0 °C), and protonic transport number (●) of the specimen in wet air

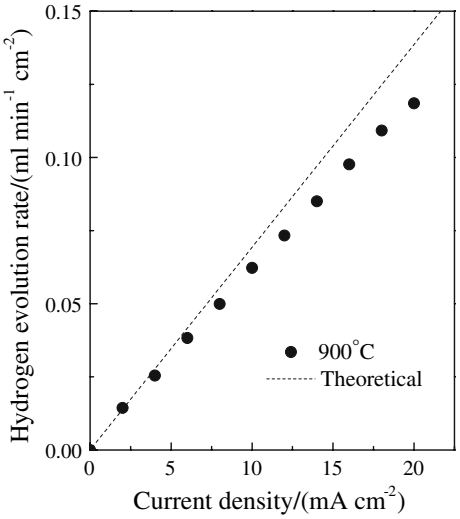

Fig. 9 Electrochemical hydrogen permeation rate of $La_{0.9}Ba_{0.1}Er_{0.85}Mg_{0.15}O_{3-\alpha}$ at 900 °C

To verify the proton conduction in the specimen directly, we performed an electrochemical hydrogen permeation (hydrogen pumping) experiment. The hydrogen evolution rate as a function of current density at 900 °C is shown in Fig. 9. The dash line stands for theoretical rate (v_{th}) worked out from Faraday's law, and the solid dot represents the observed rate (v). The protonic transport number (t_{H}) can be calculated from the ratio of the observed rate versus the theoretical rate to be 0.86. From Figs. 6 and 5, the total ionic (protonic and oxide ionic) transport number is unity at hydrogen atmosphere and low oxygen partial pressure, therefore, oxide ion transport number is 0.14 at 900 °C.

Conclusion

Doubly doped perovskite-type $La_{0.9}Ba_{0.1}Er_{1-x}Mg_xO_{3-\alpha}$ ($x = 0.05, 0.1, 0.15, 0.20$) ceramics were synthesized by high temperature solid-state reaction. The conductivity of these specimens changed with the atmosphere, temperature, and quantity of the dopant. The conductivity in H_2O–Ar was higher than that in D_2O–Ar, which showed the isotope effect and the essence of proton conduction at water vapor atmosphere. The ceramics specimen was an ion (proton and oxide ion) conductor at low oxygen partial pressure and a mixed conductor exhibiting oxygen ion, proton, electron hole conduction at high oxygen partial pressure for example, in air. It was mainly an ion conductor in hydrogen atmosphere and a mixed oxygen ion and electron hole conductor at high dry oxygen-containing atmosphere. The conductivity was dominated by oxide ion

at 500 °C, however, the dominated defect type transfer to electron hole above 600 °C in dry oxygen-containing atmosphere. The total conductivity for different atmosphere proceeded in this order: air > wet air > wet H_2. Among the specimens determined, $La_{0.9}Ba_{0.1}Er_{0.85}Mg_{0.15}O_{3-\alpha}$ showed the highest conductivity (4.3×10^{-3} Scm^{-1} at 1000 °C) which was higher than the conductivity (8.8×10^{-4} Scm^{-1} at 1000 °C) of $La_{0.9}Ba_{0.1}ErO_3$ in wet hydrogen, owing to the more electron holes concentration of doubly doped specimen.

Acknowledgement This work was supported by the National Natural Science Foundation of China (No. 20771079)

References

1. Iwahara H, Esaka T, Uchida H, Maeda N (1981) Solid State Ionics 34:359
2. Iwahara H, Uchida H, Ono K, Ogaki K (1988) J Electrochem Soc 135:529
3. Yajima T, Kazeoka H, Yogo T, Iwahara H (1991) Solid State Ionics 47:271
4. Liang KC, Nowick AS (1993) Solid State Ionics 61:77
5. Larring Y, Norby T (1994) Solid State Ionics 70–71:305
6. Shimura T, Komori M, Iwahara H (1996) Solid State Ionics 86–88:685
7. Murugaraj P, Kreuer KD, He T, Schober T, Maier J (1997) Solid State Ionics 97:1
8. Fujii H, Katayama Y, Shimura T, Iwahara H (1998) J Electroceram 2:119
9. Ma GL, Zhang F, Zhu JL, Meng GY (2006) Chem Mater 18:6006
10. Iwahara H, Asakura Y, Katahira K, Tanaka M (2004) Solid State Ionics 168:299
11. Marnellos G, Stoukides M (1998) Science 282:98
12. Iwahara H, Shimura T, Katahira K, Masahiro T (2000) Electrochemistry 68:154
13. Ma GL, Shimura T, Iwahara H (1998) Solid State Ionics 110:103
14. Iwahara H (1996) Solid State Ionics 86–88:9
15. Iwahara H (1988) Solid State Ionics 28–30:573
16. Potter AR, Baker RT (2006) Solid State Ionics 177:1917
17. Nowick AS, Du Y (1995) Solid State Ionics 77:137
18. Hibino T, Mizutani K, Iwahara H (1993) J Electrochem Soc 140:2588
19. Shimura T, Esaka K, Matsumoto H, Iwahara H (2002) Solid State Ionics 149:237